Prediction of the Fillet Mass and Topology of Aluminum Brazed Joints

Numerical modeling can foretell the features and acceptability of brazed structures

BY D. P. SEKULIC, F. GAO, H. ZHAO, B. ZELLMER, AND Y. Y. QIAN

ABSTRACT. The topology of brazed joints can be predicted *a priori* with minimal empirical input. It is demonstrated that when one predicts with sufficient precision the mass of filler metal destined to flow into the joint zone, joint topology can be determined with assurance by using the proposed methodology and numerical modeling using a finite element code. The numerical approach to determination of brazed joint topology is based on the principle of minimum potential energy of the equilibrium membrane of the molten metal at the onset of solidification. The theoretical predictions of fillet mass and joint shapes are corroborated with experimental data, and independently with the numerical predictions obtained using general-purpose *Surface Evolver* interactive software. The predictions of the numerical modeling indicate not only whether or not the joint formation would likely be acceptable vs. the selection of materials and process parameters, but also all the important geometrical features of a joint and data necessary for determination of mechanical and thermal integrities of various brazed structures. Without an empirical input, best results are obtained when the residual layer is predicted by using a nonequilibrium assumption for modeling the clad melting prior to flow. If the empirical input is utilized, the best results are obtained when the residual layer is measured in situ.

Introduction

In manufacturing aluminum compact heat exchangers, controlled atmosphere brazing (CAB) has been the process of choice (see section on Brazing Conditions and Materials for details). However, related designs of aluminum brazing sheets (sheet gauge, clad ratio, material compositions) and, in particular, the determination of the optimal shapes of the mating joint surfaces of the joint zone in actual designs (that have become increasingly intricate) have mostly been based on empirical data. Reliable analytical or numerical tools developed solely for prediction of the joint topology, and, specifically, for an assessment of the likelihood that the joints will be sufficiently good, still do not exist. To accomplish such a goal in an efficient manner, one needs a good understanding of related phenomena during the brazing process. In fact, a key requirement is to establish mass balance "links" between 1) the initial state and composition of the brazing sheet, 2) the brazing process parameters, and 3) the molten clad filler metal state at the onset of solidification. The molten clad mass that will flow and form the brazed joint represents only a fraction of the available mass prior to brazing. Our experimental results have revealed that the mass flow rate of the molten clad/filler depends heavily on the following set of parameters (Refs. 1, 2): 1) silicon content in the clad and the substrate composition, 2) cladding ratio, 3) ramp-up rate during the heating segment of the brazing cycle, 4) peak brazing temperature, and 5) flux coverage, in addition to other process and material characteristics/conditions (to be kept fixed and/or under control).

In Fig. 1, cross-sectional views of actual single and multiple brazed joints are presented. It should be noticed that the mating surfaces involved have both flat and curved shapes. In addition, some of them may be strongly three-dimensional (such as the joint at the far right of Fig. 1B, the 3-D features of which are not clearly visible in the 2-D image). All the brazing sheet surfaces (in Fig. 1, these are labeled Mating Surfaces B and C; a brazing sheet schematic before forming and exposure to brazing is presented in Fig. 2A) are covered with distinct residue layers (both far from and close to the joints). See Fig. 2B for a schematic representation of the residue location vs. the joint zone. In addition, these residue layers are more or less uniform. The nonuniformity, if present (see, for example, the area midway between the edges of the curved convex Surface B in Fig. 1B), is most often a consequence of the trade-offs among 1) metal forming of the originally flat clad sheet material (which prior to brazing usually leads to a clad layer thinner at convex and thicker at concave surfaces), 2) the curvature effects of surface tension driven flows that take place during brazing, and 3) local reactive and diffusion phenomena during dwell at the peak brazing temperature. Our goal is to predict with reasonable accuracy the clad distribution and the joint shape after solidification.

In this paper, results of a comprehensive study of the joint shape topology, formed under tightly controlled brazing conditions, are presented. The organization of the paper is as follows. First, the brazing process conditions and materials under consideration are listed. The relationship between the joint zone and the residue-clad layer is discussed next. Subsequently, two models of the clad mass and related joint topology formation are discussed in detail. Finally, the predictions of shape topologies of a series of joints typical for aluminum compact heat exchanger designs (i.e., tube-fin, tube-manifold, etc.) are illustrated and the corresponding prediction deviations summarized by comparing predictions and actual designs.

KEY WORDS

Aluminum Brazing
Heat Exchangers
Controlled Atmosphere Brazing
Numerical Modeling
Brazed Joint Topology

Brazing Conditions and Materials

All the brazing experiments were executed following the state-of-the-art CAB technology in a high-purity nitrogen (99.999%) atmosphere. The rapid-quench

D. P. SEKULIC and H. ZHAO are with UK Center for Manufacturing, University of Kentucky, Lexington, Ky. F. GAO is currently with Collaborative Research Center for Advanced Science and Technology, Osaka University, Osaka, Japan. Y. Y. Qian is with National Key Laboratory of Advanced Welding Production Technology, Harbin Institute of Technology, Harbin, China. B. ZELLMER is with the Department of Mechanical and Industrial Engineering, Marquette University, Milwaukee, Wis.

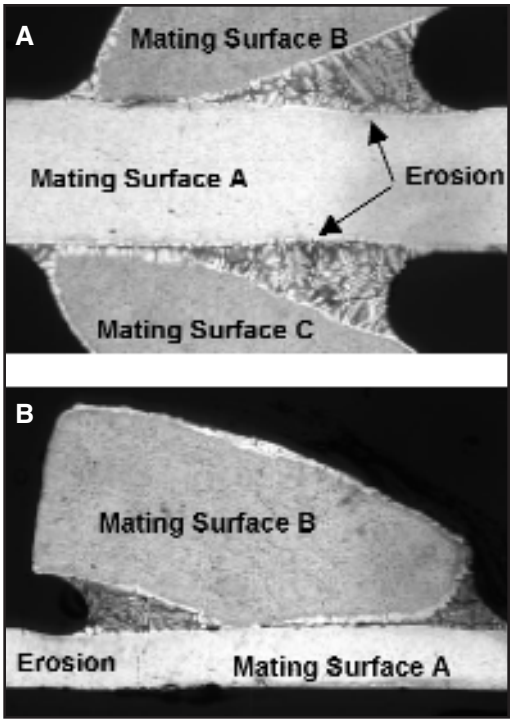

Fig. 1 — Cross-sectional views of a brazed joint. A — A configuration featuring multiple joints in a compact heat exchanger; B — a manifold extruded tube double-sided single joint. Detailed information about process conditions and materials is given in Ref. 3.

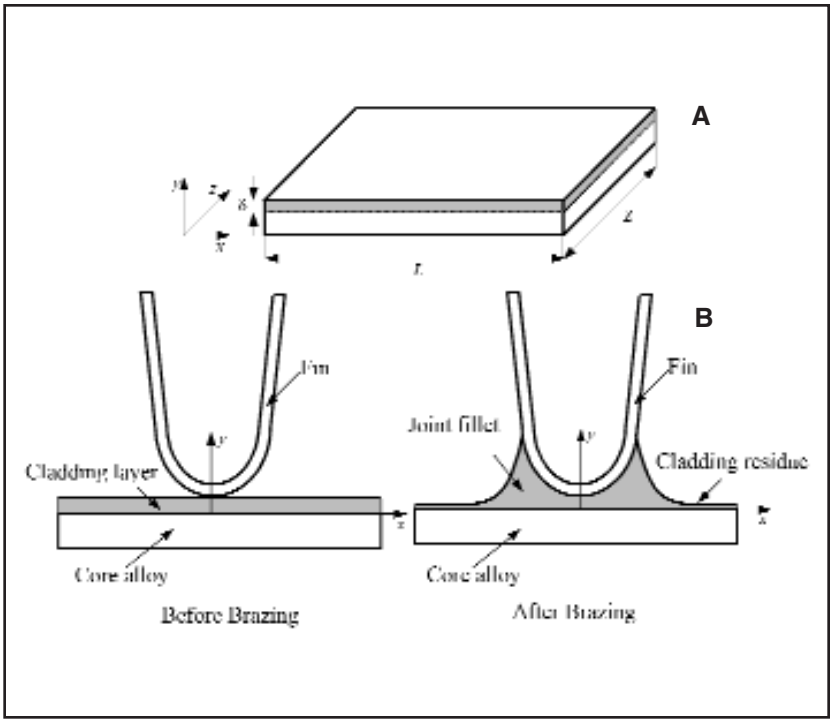

Fig. 2 — Schematics of: A — a brazing sheet ($\delta = \delta_{clad}$ denotes cladding thickness and L and Z the 2-D length dimensions of the brazed joint corresponding sheet area); B — a compact heat exchanger fin-tube joint formation before and after brazing — a basic topology.

was accomplished first by a forced convection of 99.9% nitrogen stream, followed by a free convection cooling, in nitrogen and, subsequently, in air, to room temperature. The margin of temperature variation at a high temperature level (i.e., 596°–607°C) was maintained around ±0.5 K. The uncertainty of temperature measurements was less than 0.2 K with a resolution of 0.1 K. Oxygen concentration during the brazing process was kept at the level of less than 100 ppm, and the dew point below –40°C.

In this study, three kinds of samples were prepared: 1) inverted wedge T joints — one member base made of a AA4343/AA3003 brazing sheet (Fig. 2A; see also Figs. 5 and 6 later), the other member made of AA3003 sheet; 2) fin-tube joints (see Fig. 2B for a schematic); and 3) manifold-tube joints of a compact aluminum heat exchanger center core (see Fig. 1). The clad ratio of the brazing sheets used in this investigation was about 10%. The manifold-tube joint samples were taken from a typical condenser featuring extruded tubes with microchannels and multilouver fins (Ref. 3). For a fin-tube joint, the actual geometry consisted of mating surfaces representing aluminum extruded tubes with 16 microchannels (with a width of 18 mm and external thickness of 1.3 mm) and a thin fin foil sandwiched between two successive tubes (for more details about the construction details of such heat exchanger cores consult Refs. 3 and 15.) The multilouver fin foil features a width of 18 mm, and a thickness of about 0.1 mm. Material of the tubes was an aluminum Alloy SD-249 with less than 0.3 wt-% Si and less than 0.4 wt-% Mg. The fin foil was made of a double-clad alloy, i.e., AA4343/AA3003/AA4343. The manifold-tube joints were assembled by using the double-side brazing sheet on the manifold shell side. The inverted wedge-T brazed joints were prepared in the form of plain coupons (base) with one side AA4343 clad and with an additional AA1145 clad on the opposite side of the sheet not involved in the brazing process. Overall dimensions of brazing sheet coupons were $25 \times 57 \times 0.38$ mm. Chemical composition of AA4343 in various cases was slightly different, but in all the considered cases it contained around 7 wt-% Si. Before brazing, the samples were ultrasonically cleaned and rinsed in acetone. Potassium fluoroaluminate flux was sprayed on surfaces with flux density in the range of 5–10 g/m^2. The experiments were performed at a peak brazing temperature of around 605°C, with dwell times of between 2 and 5 min. The solidus and liquidus temperatures of the clad material were around 577° and 615°C, respectively. The typical brazing process temperature history is shown in Fig. 3. It should be mentioned that, although the proposed methodology is developed for CAB Nocolock™ technology, the same approach may be extended to other brazing technologies (Ref. 7).

Residue Clad Layer and a Relationship with the Brazed Joint Area — Empirical Evidence

It is a well-known fact (gained through numerous empirical accounts) that a brazing process involving brazing sheets always features a residue clad layer at locations away from joint zones. This is an inherent clad-core interface phenomenon, occurring due to a reactive flow of molten clad over the substrate, and, in particular, as a consequence of a significant presence of Si diffusion, both prior to and during clad melting, mushy phase formation, and resolidification. Generally, the thickness of the clad residue layer is more or less uniform if 1) the interface is flat, 2) the clad layer that produces melt destined to flow into the joint is of a limited extent (as, for example, in the case of fin-tube joints with a small fin-pitch length), and 3) the heat and mass transfer conditions are kept uniform. Surface tension and gravity are the dominant driving forces for the associated clad flow if the optimal surface conditions are achieved (an adequate flux presence, i.e., good wetability, and small substrate dissolution). Although one may hope to determine the ultimate state of the molten clad

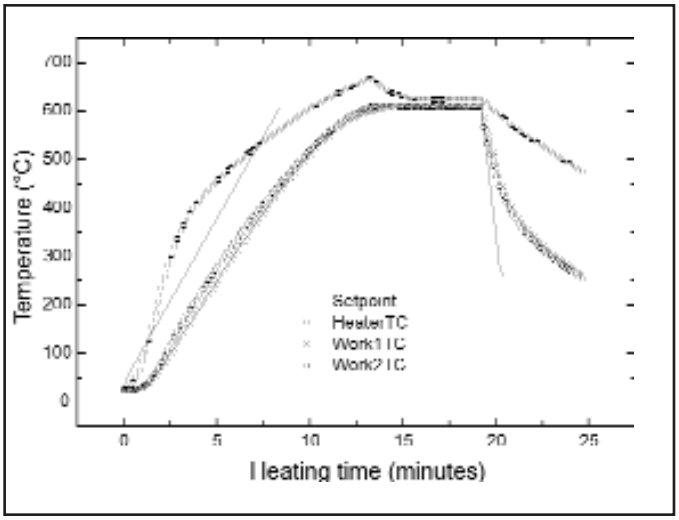

Fig. 3 — A typical ramp-up/dwell/quench temperature history of a CAB brazing process.

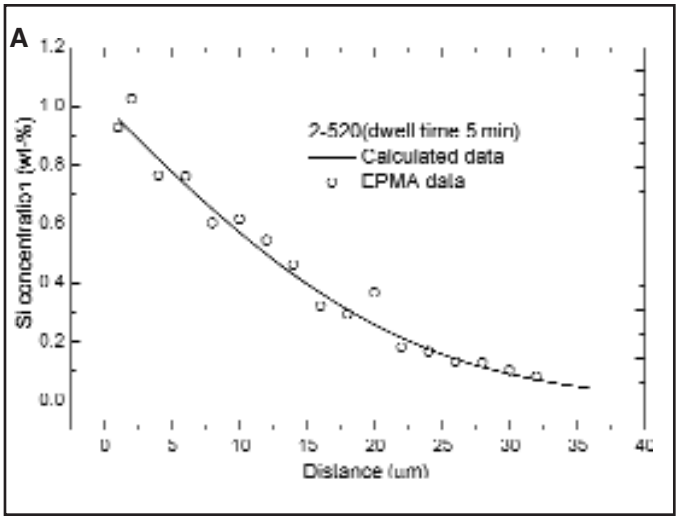

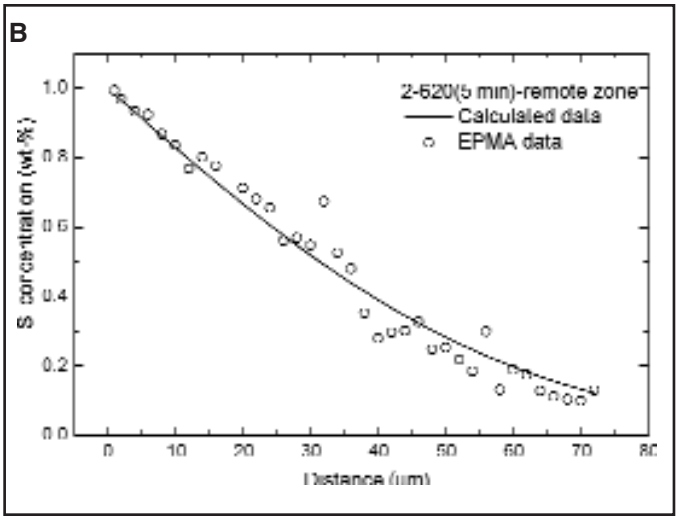

Fig. 4 — Silicon diffusion at the clad-substrate interface. A — No melting at 520°C, dwell time 5 min; B — a brazing process at 620°C, dwell time 5 min, residue location far from the joint zone. Alloys: core/clad AA3003/AA4343. For details of the diffusion patterns, see Ref. 1.

at the onset of solidification by studying the model of the reactive flow phenomena, it is very hard to simulate the dynamics of the clad flow because of the complexity of nonlinear, transient, and spatially distributed transport processes (Ref. 4). Until recently, only fully empirical and/or semiempirical approaches to determination of molten clad and joint formations were available (and these already in use for some time, Ref. 5). Therefore, the clad mass that would form the desired brazed joint could not be determined *a priori* by a deterministic modeling approach alone, without involving a significant empirical input, say through the introduction of the flow factor (Ref. 5).

One may try to predict the mass of the clad that will flow by modeling the clad flow as an independent heat and mass transfer process, involving the complex dynamics of spatiotemporal phenomena that follow such a reactive flow, hoping that the radical set of assumptions needed to make the corresponding mathematical model palpable will work within a reasonable margin of error (Ref. 6). However, one will encounter problems not only with the plausibility of the adopted assumptions, but also because the thermophysical properties of both the analyzed fluid and substrate interface state are unknown. Such an approach, when, as in soldering and brazing, the reactive flow conditions and process parameters are imposed, is very difficult to formulate and may be beyond the reach of existing theories (Ref. 4). In the approach suggested in this paper, however, we consider quite a different way to resolve this problem.

Instead of modeling the dynamics of the clad flow, we try to determine the residue layer mass first; then, based on the conservation of mass principle (along with a radical idealization regarding the minor influence of substrate dissolution and subsequent erosion) we determine the mass of liquid clad to flow to a joint as a balance between the initial and final masses of the clad layer. As our studies have indicated (Refs. 1, 2), such an approach would work reasonably well if the brazing parameters are selected to be optimal, and if the 3-D effects are not significant. But "reasonably well" is not necessarily sufficient. One of the objectives of this paper is to explore how good such assumptions actually are. The question is not whether the margin of error would exist — since it always will — but whether such a margin of error is small enough to provide reasonable guidelines for effective joint design, eliminating as much as possible the very costly and time-consuming test trials otherwise necessary for final selection of the process parameters. A detailed description of the CAB process parameters and a comparison with the other options are given in Ref. 7.

Prediction of the Molten Clad Mass at the Onset of Solidification and the Joint Topology

The joint formation models proposed in this paper are based on a prediction of the residue layer mass formed at surfaces after the brazing process. In this study, 3-D effects (such as those caused by nonuniform clearance) will be neglected. The following main hypothesis is adopted: *The mass of clad needed to form a joint is equal to an algebraic sum of contributing masses formed from the available clad mass by transport mechanisms present during the melting and flow phases of the brazing cycle, i.e., the joint mass is equal to the initial clad mass reduced by the mass of the residue.*

The various contributions to the total mass should be determined by taking into account: 1) formation of a silicon-depleted layer within the clad at the interface between the clad and substrate prior to clad melting, 2) the solid fraction formed in the semisolid mushy state of the clad upon melting at the peak brazing temperature (a liquid locked within the solid microstructures), and 3) the initial mass of clad prior to the brazing process.

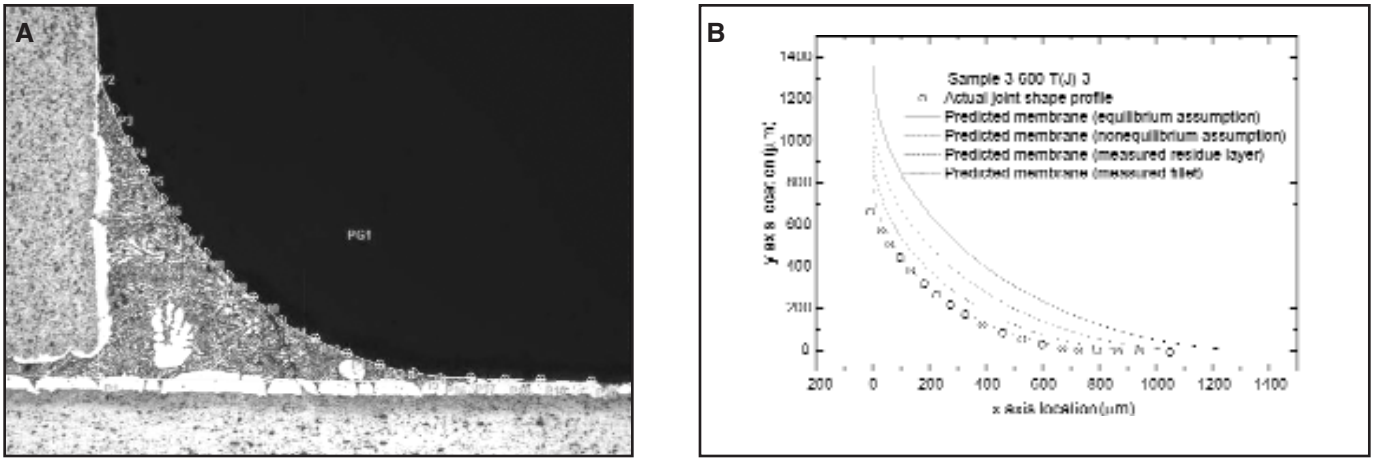

Fig. 5 — An inverted wedge-T joint. Brazing conducted at the peak brazing temperature of 600°C, dwell time 5 min. A — Actual brazed joint shape profile. B — Comparison between predicted and experiment data describing the joint topology. Predictions via 1) equilibrium phase diagram assumption, 2) nonequilibrium model of melting, 3) measurement of the residue, and 4) measurement of the fillet cross-section area.

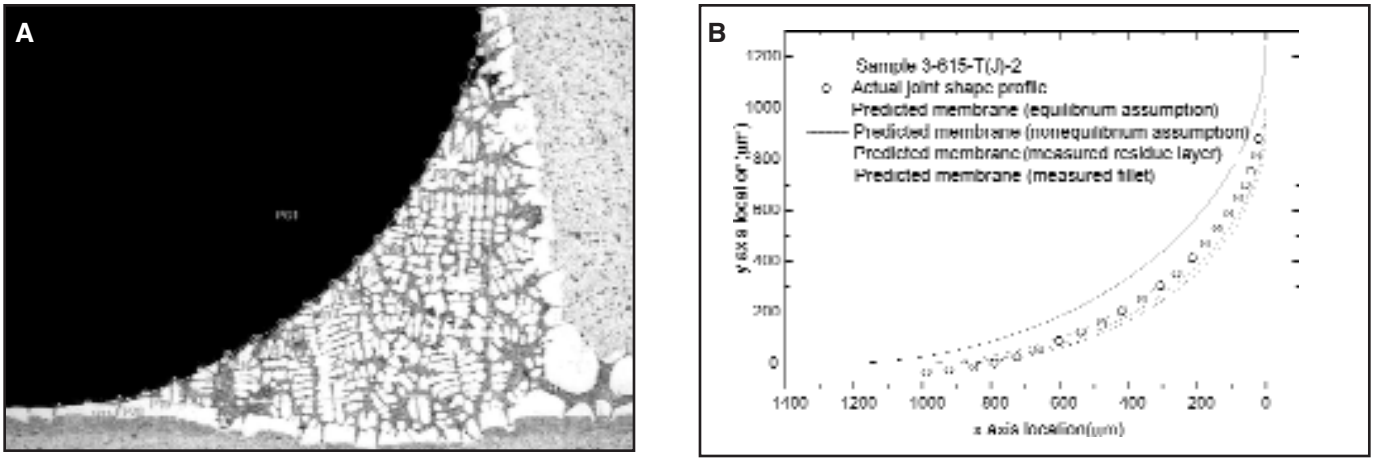

Fig. 6 — An inverted wedge-T joint. The peak brazing temperature at 615°C, dwell time 5 min. A — Actual brazed joint shape profile. B — Comparison between predicted and experiment data describing the joint topology. The prediction methods as indicated in Fig. 5.

The key problem in determining the contributions of 1 and 2 is not so much achieving an understanding of related physical mechanisms that follow their formation, but eliminating the need to depend on empirical data involving formation of residue (e.g., flow factor, Refs. 5, 8). So, our goal is to explore how far one can go in reducing the difference between the best prediction and the actual joint size solely by utilizing proposed models, without involving empirical data regarding the flow factor.

In order to make this problem solvable, the following assumptions should be put forward:

1) The densities of all phases are considered as constant. Therefore, the volume changes during melting and/or solidification (shrinkage) would not influence the final results.

2) The clad alloy phase change occurs either under equilibrium or nonequilibrium conditions. Therefore, in the first case, the phase diagram of an Al + Si system can be used to analyze the development of the α-Al solid phase and the Al-Si liquid based on a "lever rule"; or, in the second case, a diffusion-controlled melting must be taken into account to determine solid fraction during melting.

3) The clad mass that flows and forms brazed joints is assumed to be equal to the mass difference between the original brazing sheet clad mass (taken as an initial condition), and the predicted/measured residue clad mass.

4) The solid phase from the mushy zone at the peak brazing temperature is evenly distributed and separated from liquid after molten filler flowed to the joint zone.

5) Mechanical deformation of the sheets (with or without cladding) and its influence on non-even clad layer distribution prior, during, and after brazing could be ignored. To ensure that no deformation of any kind takes place during the sample preparation, a vacuum impregnation has been conducted at room temperature, and the resin hardening is conducted at atmospheric pressure and temperature.

6) The erosion of the substrate alloy was assumed not to influence (even if present) the final equilibrium membrane shape of the molten metal free surface at the onset of solidification. This assumption requires a precise targeting of the peak brazing temperature and good temperature uniformity of the sample during brazing. These conditions can be controlled more easily under laboratory conditions (as was done in our case), but almost never fully under actual brazing conditions, unless the brazed structure has a small total mass and a simple configuration.

The components of the mass balance are as follows. The ultimate mass of the clad in a joint is defined as

$$\begin{aligned} m_{joint} &= \delta_{equivalent} \times LZ\rho \\ &= m_{clad} - m_{residue} \\ &= m_{clad} - \left(m_{depleted} + m_{solid} + \sum_{i=3}^{n} m_i \right) \end{aligned} \quad (1)$$

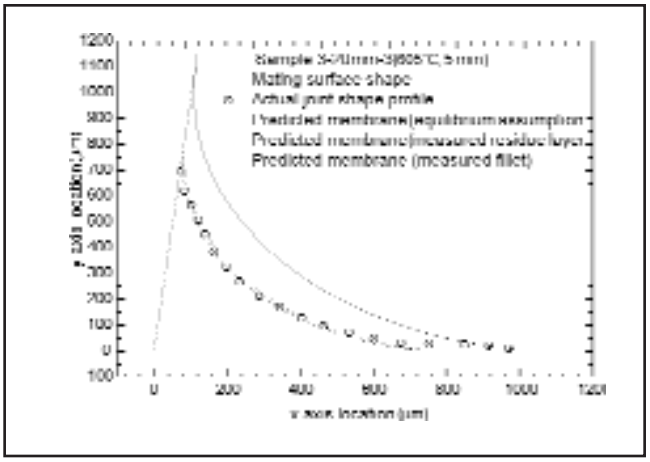

Fig. 7 — An inverted wedge-T joint with nonorthogonal mating surfaces taken into account for the equilibrium membrane prediction. The peak brazing temperature at 605°C, dwell time 5 min. Comparison between predicted (see Fig. 5 caption for details) and experiment data describing the joint topology.

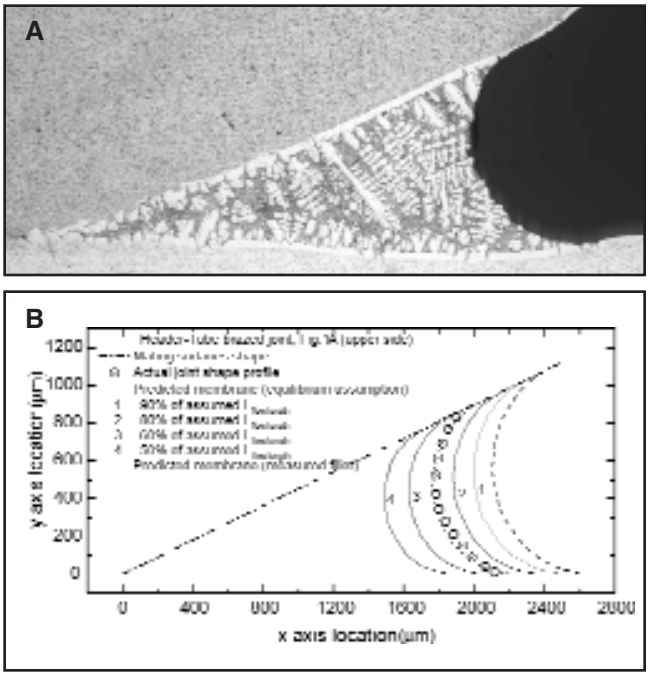

Fig. 8 — Header-tube brazed joint, side B, see Fig. 1A. A — Actual brazed joint. B — Comparison between an actual joint profile and the predicted topology. The influence of the clad flow length.

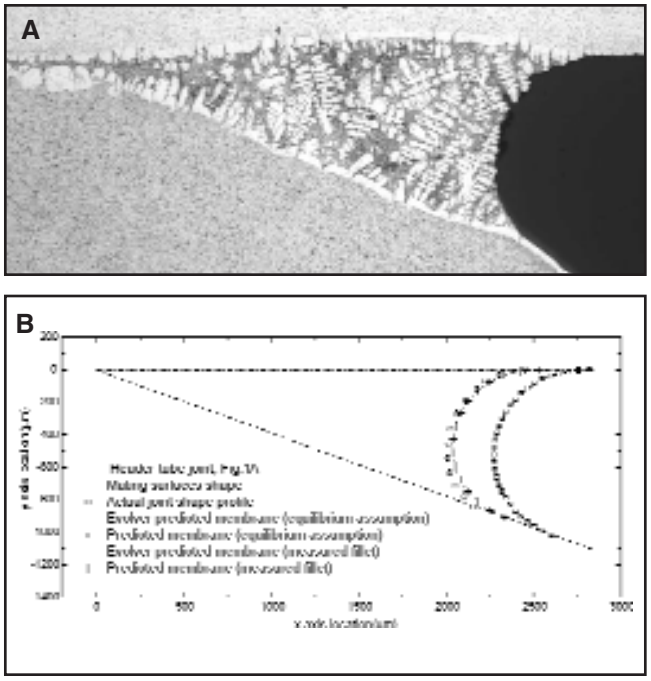

Fig. 9 — Header-tube brazed joint, side C, see Fig. 1A. A — Actual brazed joint. B — Comparison between an actual joint profile and the predicted topology. Comparison with Evolver calculations.

where m_{clad} represents the clad mass before melting, $m_{depleted}$ is the mass of the Si-clad-depleted zone at the clad-substrate interface at the onset of the peak brazing temperature, m_{solid} is the solid fraction of the clad mushy zone melt assumed not to flow, and m_i, i=3,…n represents the other not-yet-specified contributions (caused by viscosity effects, shrinkage, etc.). The simple schematic of a brazing sheet featuring overall dimensions as listed in Equation 1 and the related coordinate system are presented in Fig. 2A, while an example of a joint formation is presented in Fig. 2B. The mass of the clad in a joint can be determined, based on the above-indicated assumptions, as a product of the clad volume (destined to flow toward a joint zone), $\delta_{equivalent} \times LZ$ and alloy density, ρ. For a uniformly distributed clad, this volume, as indicated above, is proportional to the brazing sheet surface area, LZ, associated with the considered joint and the thickness of the molten clad at the onset of flow, $\delta_{equivalent}$, that is,

$$\delta_{equivalent} = \delta_{clad} - \delta_{residue} \qquad (2)$$

The clad thickness defined by Equation 2 represents an equivalent thickness of the clad to flow (i.e., the portion of the total clad mass divided by clad density that will ultimately end up in the adjacent joint). It is assumed that the equivalent molten layer thickness, Equation 2, may be predicted as a difference between the initial clad thickness and the ultimate residue formation thickness. The goal is to theoretically predict (i.e., not necessarily to measure *a posteriori*) the residue formation. The initial clad thickness, δ_{clad}, is known precisely *a priori* for a given sheet gauge δ_{sheet} and the cladding ratio, conveniently expressed as a fraction, C_R. Therefore, the clad thickness is as follows.

$$\delta_{clad} = \delta_{sheet} \cdot C_R \qquad (3)$$

The residue-clad thickness, $\delta_{residue}$, in Equation 2 is an important contribution of the mass balance that must be *a priori* predicted. The key assumption here is to adopt additiveness of the contributions to the residue mass (i.e., the residue thickness for a 2-D uniformly distributed mass and constant density). In other words,

$$\delta_{residue} = \delta_{diff} + \delta_{solidsolution} + \sum_{i=3}^{n} \delta_i \qquad (4)$$

The first term on the right-hand side in Equation 4 is a contribution to the residue thickness caused by solid-state diffusion prior to melting and formation of a Si-depleted zone of the clad at the clad-substrate interface (Ref. 1).

The last term in Equation 4 represents a set of equivalent residue-formation-contributing-thicknesses in excess of the first two dominant terms, and is related to the last term in Equation 1. These contributions account for the influences of eventual molten metal viscosity effects, a reaction flow of molten clad over the core

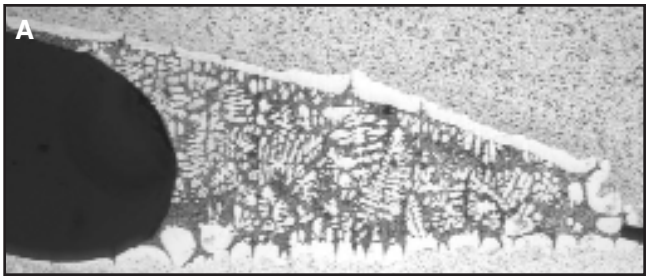

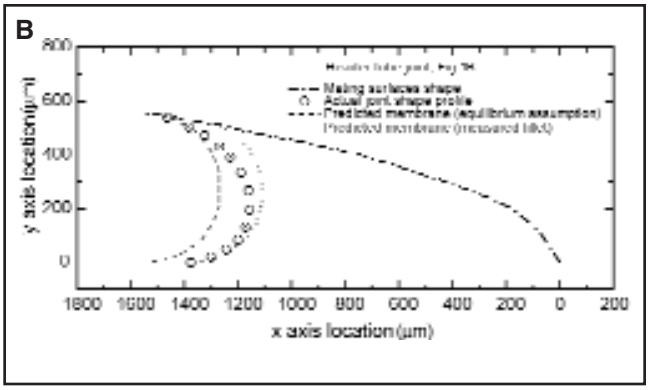

Fig. 10 — Header-tube brazed joint (cross section parallel to tube channels), see Fig. 1B. A — Actual brazed joint. B — Comparison between an actual profile and the predicted topology.

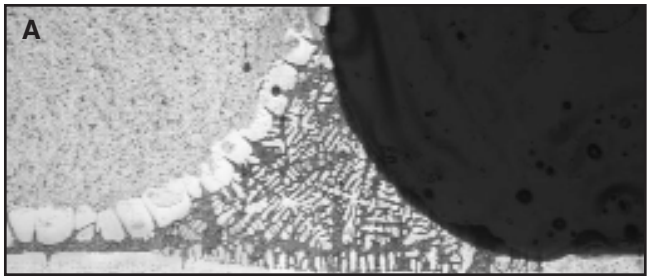

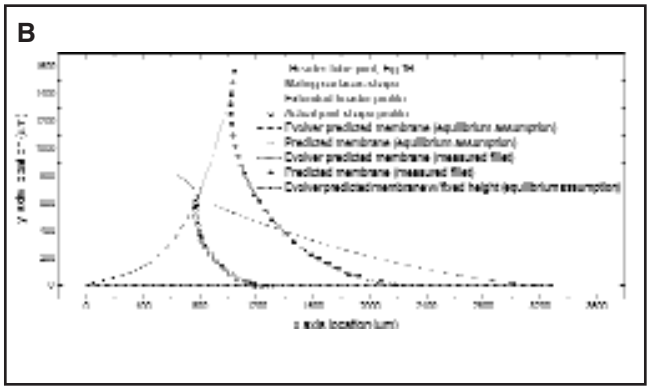

Fig. 11 — Header-tube brazed joint (cross section parallel to the tube channels), see Fig. 1B. A — Actual brazed joint. B — Comparison of an actual 3-D profile and the predicted real and hypothetical 2-D topology.

substrate, shrinkage effects, etc. (In this study these contributions are assumed to be negligible.) Upon reaching a certain elevated temperature level (T_{diff}) during the ramp-up heating (with the ramp rate $\partial T/\partial t$) the diffusion becomes sizable and reduces the amount of clad alloy to be melted. For a 2-D layer configuration (the condition satisfied due to the fact that $\delta_{clad}/L_{flow} << 1$), the corresponding mass per unit area of the surface can be determined as $\delta_{diff}\,\rho$, where

$$\delta_{diff} = \mathbf{C}\left(\frac{D(T_{peak} - T_{diff})}{(\partial T/\partial t)_{ramp}}\right)^{\frac{1}{2}} \frac{c_{Si,o}}{c_{Si,i}} \qquad (5)$$

In Equation 5, **C** is a constant factor, (its physical significance is described in Ref. 5), D is the diffusion coefficient for Si in the solid substrate, and $c_{Si,o}$ and $c_{Si,i}$ represent Si solid solubility in the aluminum-silicon alloy at a given temperature, and the initial silicon content, respectively. Note that $(T_{peak} - T_{diff})/(\partial T/\partial t)_{ramp}$ is proportional to the diffusion time. So, we determine this time knowing the materials' properties, peak brazing temperature, and heating ramp rate prior to joint formation.

The mass of the clad per unit surface area $\delta_{solid\ solution}\,\rho$, assumed to stay within the residue layer due to formation of the solid solution in situ, can be determined by defining $\delta_{solid\ solution}$ as follows.

$$\delta_{solidsolution} = \left(\delta_{Sheet} C_R - \delta_{diff}\right) f_{solid} \qquad (6A)$$

$$f_{solid} = \begin{cases} f_{equilibrium} = \dfrac{c_{Si,liq} - c_{Si,i}}{c_{Si,liq} - c_{Si,sol}} \\ \text{for an equilibrium assumption.} \\ \\ f_{nonequilibrium} = \left(\dfrac{r}{R}\right)^3 \\ \text{for a nonequilibrium assumption.} \end{cases} \qquad (6B)$$

Equation 6 indicates that two models of melting should be considered. In the case of the validity of equilibrium conditions, i.e., the validity of the phase diagram for Al-Si alloy phase distribution (in our case AA4343), the solid fraction in the melt at the onset of flow can be calculated using the lever rule (see Equation 6B for an equilibrium assumption). Here, $c_{Si,liq}$, $c_{Si,i}$, and $c_{Si,sol}$ represent the silicon solubility at the liquid α-Al state, initial silicon content in the Al-Si alloy under consideration, and silicon solubility at the Al-Si solid state, respectively. Alternately, the solid fraction may be estimated by using Equation 6B for a nonequilibrium assumption model. This quantity has, in that case, to be determined based on a study of a diffusion-controlled melting (Ref. 14). The value of $f_{nonequilibrium}$ should then be calculated numerically as a cubic ratio of the following: 1) the length scale of the grain of the partially melted grain at a state of the Si diffusion level that corresponds to the Al alloy solidus, but at the given peak brazing temperature, r in Equation 6B; and 2) a length scale of the initial grain size prior to melting, R in Equation 6B. This calculation takes into account nonlinear Si diffusion during melting to define r, but the details of this aspect of calculation are beyond the scope of the present paper and may be found in Ref. 14.

One of the main objectives of the present study is to establish whether a simple equilibrium assumption model can be used reliably, or if a more elaborate approach involving both melting and solidification studies is needed. It will be shown that the former assumption, originally introduced by Terril (Ref. 5), may work well only if a significant empirical input through the flow factor is taken into account. Hence, the newly proposed nonequilibrium melting model would provide a significantly better result if no empirical input is available

Finally, the thickness of the clad that will flow into the joint from the adjacent surface area LZ can be determined from

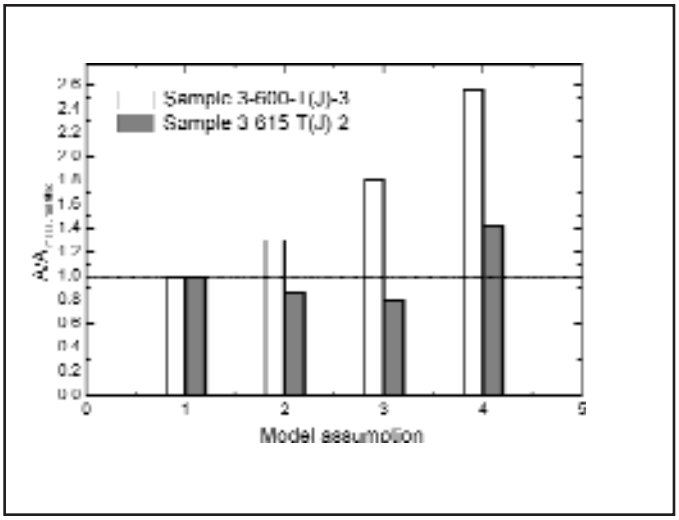

Fig. 12 — Comparisons of the predicted and measured fillet size areas (A = fillet size): 1) measured fillet, 2) measured residue layer size, 3) nonequilibrium assumption, and 4) equilibrium assumption.

the equation as follows:

$$\delta_{equivalent} = \frac{m_{joint}}{LZ\rho} = \frac{1}{Z}\int_{joint\ area} ydx = \delta_{Sheet}C_R - \left(\delta_{diff} + \delta_{solidsolution} + \sum_{i=3}^{n}\delta_i\right) \quad (7)$$

In Equation 7, terms of the sum $\sum_{i=3}^{n}\delta_i$ may be, in principle, positive, negative, or equal to zero. If no other contributions are taken into account (in addition to the ones determined by Equations 5 and 6), this sum is equal to zero. In any case, in our considerations, this term will be assumed to be equal to zero. Hence, any contributions due to the viscosity, friction, shrinkage, and erosion would be neglected. These influences will be considered elsewhere.

Two additional issues must still be mentioned. If the clad mass distribution is uniform (a condition that may be considered as satisfied when state-of-the-art brazing sheets are considered), the unit length in z direction replaces a need to have the magnitude Z separately determined (assuming that 3-D effects can be neglected). Determination of the related clad layer length L is a much more difficult issue to resolve. As will be discussed later, the magnitude of the predicted joint formation directly depends on the magnitude of the so-called clad flow length, L_{flow}, which will be identical to L in this case. This entity can easily be determined in some cases (such as a fin-tube joint when a half of the fin pitch clearly represents the clad flow length because of the symmetry of the neighboring joint zones). If the closest neighboring joint is remote, the clad flow length may be significantly influenced by the effects to be included in the summation term in Equation 7. Otherwise, the prediction of the mass of clad to be accumulated in a joint may be either over- or underpredicted (see section on Header-Tube Brazed Joint).

Silicon diffusion into the substrate alloy across the clad-substrate interface prior to the clad melting influences the silicon composition both in the clad and the substrate; hence, the proper selection of the diffusion coefficient D (see Equation 5) is of a paramount importance. It was recently demonstrated (Ref. 1) that the diffusion coefficient must be determined if possible in situ (meaning for a particular sample/material under consideration and not adopted from literature data) if a reasonable prediction of the clad residue is to be accomplished. The classic Fick's second diffusion law written for a diffusion into the semi-infinite medium (a good approximation in this case due to a relatively small ratio of the brazing sheet thickness to the diffusion path length) can be written as follows:

$$\frac{\partial c}{\partial t} = D\frac{\partial^2 c}{\partial x^2} \quad (8)$$

with the boundary and initial conditions $c = 0$ at $x = \infty$ and $t > 0$; $c = 0$ at $t = 0$ and any x; and $c = c_0$ at $x = 0$ and $t > 0$. So, a simple distribution of Si concentration would suffice for our analysis.

$$c_{(t,x)} = c_0 \mathrm{erfc}\left(-\frac{x}{2\sqrt{Dt}}\right) \quad (9)$$

In Fig. 4, experimental data for Si concentration profiles in the core close to the interface of considered samples (AA3003) are summarized for a case of the peak dwell temperature still below the Al + Si solidus (Fig. 4A) and after brazing conducted at the peak brazing temperature (Fig. 4B). It can be concluded that the diffusion profiles illustrate very good agreement with assumed idealizations, and that the resulting diffusion coefficients determined from these data (Ref. 1) fit very well with the concentration profile. The so-determined diffusion coefficients were utilized in Equation 7 to determine the residue thickness.

Upon determination of the mass of clad destined to reach the joint zone, a determination of the joint topology was based on a computer simulation of the joint shape governed by surface tension and gravity and constrained within the topology of the two or more mating surfaces to be joined. The developed computer software utilizes the method proposed by the authors (Refs. 9–11). The software represents an in-house finite element code used for a determination of an optimal free surface joint shape in such a way as to satisfy the minimum potential energy requirement (Ref. 10). Its advantage when compared to general-purpose software (like *Surface Evolver* [Ref. 12]) is a much more compact architecture and an easy incorporation in a specialized joint formation prediction numerical software under development (to be presented elsewhere). The approach is based on the following premise: *The topology of the joint shape is defined by an equilibrium membrane (featuring minimum potential energy) formed at the onset of solidification of the molten metal entrapped within the two or more mating surfaces in the joint zone* (Ref. 9). The free surface of the fillet is characterized by its potential energy, which must be minimal for the ultimate equilibrium state at the onset of solidification. Hence, the optimization software selects the fillet shape (an "equilibrium membrane") that corresponds to the smallest potential energy of the free molten metal surface. The potential energy of the equilibrium membrane is given by (Ref. 9)

$$E_p = E_s + E_g + E_w \quad (10)$$

where

$$E_s = \int_a \gamma da \quad (11)$$

represents the membrane surface potential energy per unit of the joint depth. Here, γ is the surface tension. In this research, the surface tension value is assumed to be constant. The second term in Equation 10, i.e.,

$$E_g = \frac{1}{L}\int_V \rho g dV \quad (12)$$

represents the gravitational potential en-

ergy of the free surface per unit of joint zone depth, where ρ is the density of the clad alloy, and *g* is the gravitational constant. The third term in Equation 10,

$$E_w = -\int_a \gamma \cos(\psi) da \quad (13)$$

represents the potential energy along the mating surface per unit area. Here, ψ is the contact angle enclosed between the tangent to a mating surface and the molten metal surface at the line of their intersection (this entity is influenced by wetting conditions). The minimization of the potential energy given by Equation 10, i.e.,

$$\min(E_p) = \min(E_s + E_g + E_w) \quad (14)$$

with respect to the membrane shape, determines the joint topology. The shape of the equilibrium surface determined by minimization of its potential energy can be conducted numerically for various imposed mating surface configurations (i.e., formed using flat surfaces [Ref. 9] or arbitrary shapes [Refs. 10, 11]).

Joint Topology — Results

The results of the predictions of joint shapes are compiled in the following two subsections. First, the results related to inverted wedge-T samples will be presented. Subsequently, the results obtained for predicting the joint topology for several types of joints taken from actual designs of heat exchangers will be discussed. The results are generated by using both an equilibrium model formulation and nonequilibrium model formulation (see Equation 6 and the discussion provided thereafter).

Wedge-T Brazed Joints

As we stated before, the wedge-T samples consisted of a horizontal brazing sheet with one-sided clad, and a vertical sheet with no clad. First, we have determined the brazed joint topology when the sheets are flat and mutually perpendicular. In Ref. 8, Woods and Robinson utilized a circle arc to fit the ultimate brazed joint profile. This approach works very well whenever the simple, flat mating surfaces with 2-D architecture are considered and when the wetting conditions are nearly ideal. However, for complex mating surfaces and poor wetting, the problem may not be so simple, and a circular arc approximation and/or "elastica curve" solution may not work. In our case, we use the inverted wedge-T samples as the benchmark geometries to verify the proximity of our predictions to the actual shapes.

In Figs. 5 and 6, a set of two samples is presented. A significant difference can be seen between the results obtained utilizing the calculated and the measured mass of the clad destined to flow into the joint. Note that a prediction procedure may be fourfold: 1) based on a measured mass/area of the given joint fillet, 2) based on a measured mass of the residue clad layer (see Equation 2), 3) based on the calculated fillet size using the nonequilibrium assumption for determination of the solid fraction, and 4) based on the calculated fillet size based on the equilibrium assumption for determination of the solid fraction of the residue. More specifically, in the considered cases (see Figs. 5 and 6), the predicted joint areas when using the equilibrium assumption were significantly larger than the ones obtained by the experiment or by using the nonequilibrium approach. In general, the magnitude of the margin of deviation and its sign depend on the method used to determine the solid fraction defined by Equation 6. If this fraction is determined based on a relaxation of the equilibrium conditions (Ref. 14), the prediction may be dramatically improved. In Fig. 5, both the equilibrium assumption model results and the nonequilibrium model results are somewhat larger than the predictions based on measurements of either the fillet size or residue layer thickness. It is obvious that the calculation of the solid fraction upon melting based on nonequilibrium melting leads to a much better agreement with the predictions based on measurements (either of the fillet area or the residue layer thickness). In Fig. 6, similarly, the worst agreement is with a prediction based on an equilibrium model. As elaborated in the section devoted to the prediction of the molten clad mass above, the nonequilibrium model takes into account the grain size scale influence and the Si-diffusion-controlled melting of a grain to determine the solid fraction at the onset of the melting termination upon reaching the solidus Si concentration within the whole grain (Ref. 14). In any case, the methodology proposed in this study for determining the fillet size based on the residue formation is sound. A deviation between the joint fillet size predictions and empirical data (regardless of whether the equilibrium or nonequilibrium melting approach is used) may be expected also because the additive terms in Equation 7 were ignored in determining the mass of the molten clad at the onset of solidification, but also (and more importantly) because no 3-D effects (say, caused by a variable clearance between mating surfaces in the z direction) are accounted for. In general, the deviation from the actual joint size may be either positive or negative, depending on local conditions and joint area topology. In cases where the empirically determined joint mass is used as an input, the results reveal that the predicted shape would have excellent agreement with the experimental data (see Figs. 5 and 6).

In a case where the erosion is pronounced, the topology of the joint may still be predicted if the mass of the eroded core is compensated for — Fig. 6. The method allows for taking into account nonorthogonal mating surfaces. The predicted results for such a case are illustrated in Fig. 7. The actual fin/tube brazed joint of the state-of-the-art compact heat exchanger design presented schematically in Fig. 2B is not necessarily in a form of a wedge-T sample. In such cases, a double-sided joint topology prediction involving curved mating surfaces should be used. (For details regarding the calculation procedures and examples, refer to Refs. 10 and 11.) These predictions lead again to an acceptable margin of deviation of the joint topology vs. the empirical data.

Header-Tube Brazed Joint

In a typical parallel aluminum compact heat exchanger, there are several different kinds of header- (manifold-) tube brazed joints. So the topology of the joint area in a given cross section may significantly differ from a simple wedge-T shape. All the samples presented here are prepared by making cross sections through joint areas parallel to tube microchannels of a real tube-header assembly. The materials and experimental procedures are described above in the section devoted to brazing conditions. The fillet size predictions to be presented in this section are established by using an equilibrium melting approach only in order to determine the maximum margins of error that may be expected in predicting the fillet mass.

In Figs. 8–11, the joint profiles of these more complicated configurations are presented. The sensitivity of the prediction to the size of the clad flow length is illustrated in Fig. 8. If the clad flow length is determined to be around 70% of the brazing sheet length associated with the joint in the given cross section, the agreement between predicted and measured joint shapes is excellent. So a reasonable margin of error can be achieved with a more precise assessment of the cladding flow length. This is not an easy task for 3-D mating surface configurations. Notice a significant erosion of the horizontal flat surface in this case. Figures 9 and 10 illustrate a reasonably good agreement between predictions and empirical data for two header-tube joints. In the case of a less-pronounced erosion, Fig. 10, the

agreement is better. In Fig. 11, a theoretical joint shape prediction is performed to establish how large the joint would be if 3-D actual mating surface configurations were reduced to a fictitious 2-D configuration. Namely, due to the specifics of the manifold design, a large available clad mass could not contribute to the joint size (one of the mating surfaces is limited in its height), and the clad merely spreads away from the joint zone. In this case the margin of disagreement between the size of the actual joint and the size of the predicted one is quite large. This example illustrates how the developed tool may be used to analyze possible design options.

In Figs. 9 and 11, the results of a comparison of the numerically predicted profiles with the ones obtained by using *Surface Evolver* (Ref. 12), a 3-D general-purpose program for surface-tension-driven phenomena (Ref. 13), and the fillet mass predictions as elaborated here are provided. When using an in-house developed software and the *Evolver* predictions for equilibrium membrane (determined using both measured and calculated mass of the clad), the predicted profiles are virtually identical. The average deviation between the two predictions (using the newly developed methodology and *Evolver* predictions) with respect to the x coordinate of the equilibrium surface for a given y location is virtually nonexistent, i.e., 0.3% and 0.1% for the measured and calculated mass/areas, respectively. The main reason for using an in-house developed software based on Equations 10–14 for this analysis is that it is tailored specifically for both single and two-sided joint formations. Namely, due to a clearance between the mating surfaces, the actual joints are never one-sided (Refs. 10, 11). The in-house developed software is equipped with an optimization routine that selects the equilibrium-free surface leading to a simultaneous minimization of the potential energy of the connected fillets.

A compilation of the margins of disagreement between theoretically determined and empirically evaluated joint areas is shown in Fig. 12 for two selected joints (see Figs. 5 and 6). From Fig. 12, one could conclude that, if the fillet mass is known, the joint topology is calculated exactly (Case 1, Fig. 12). If the calculation is based on residue mass determination, the predictions are within approximately 20% (Case 2, Fig. 12). However, if the joint zone geometry is a more intricate 3-D configuration (in particular in the presence of nonuniform clearances between mating surfaces) and if the various levels of erosion are present, predictions made by using a model based on the solid fraction determination, and assuming the equilibrium conditions, are not necessarily good (Case 4, Fig. 12). A significant improvement can be obtained if this calculation is performed following a nonequilibrium assumption (Case 3 vs. Case 4, Fig. 12).

Conclusions

In this paper, models for the determination of brazed joint topologies are elaborated. The results of various joint formation shape predictions have been compared with empirical data for inverted wedge-T and complex header- (manifold-) tube joints, typical for designs of standard aluminum compact heat exchangers.

The following conclusions can be drawn:

1) The hypothesis that the brazed joint mass can be determined by predicting the mass of the clad residue formed in vicinity of the joints even without using an empirical input (such as flow factors) is proven valid. The level of prediction precision can be improved by an additional empirical input.

2) If the mass of the clad that flows and forms a brazed joint is known *a priori*, the predicted brazed joint topology is in a good agreement with the actual joint profile for relatively simple geometries and not-sizable 3-D influences.

3) The joint topology of actual 3-D joints, such as in cases of fin-tube and header- (manifold-) tube brazed joints, can be predicted with an acceptable margin of error even if based on a limited number of dominant molten clad formation mechanisms (such as the clad layer Si-depletion at the interface and solid solution separation), if erosion and 3-D effects are not sizable and if the residue formation is known.

4) The prediction of the clad residue based on an equilibrium model of the solid fraction formation upon melting is noticeably inferior when compared to that based on a nonequilibrium formulation. Hence, the predictions of the brazed fillet size must be determined by using a nonequilibrium, Si-diffusion-controlled melting model for the residue formation.

Acknowledgments

This research work was supported by the National Science Foundation through the NSF Grant DMI-9908319 and in part by the Kentucky Science and Engineering Foundation through the grant KSEF-525-RDE-005. The authors would like to thank Dr. Ken Brakke, Department of Mathematics, Susquehanna University, for assistance regarding the use of the *Evolver* software. One of the authors (G.F.) would like to acknowledge the research assistantship obtained from the University of Kentucky Center for Manufacturing. An early version of this paper was presented at the International Brazing and Soldering Symposium, 2002 AWS Welding Show and Annual Convention, Chicago, Ill.

References

1. Gao, F., Zhao, H., Sekulic, D. P., Qian, Y. Y., and Walker, L. 2002. Solid state silicon diffusion and joint formation involving aluminum brazing sheet. *Materials Science and Engineering A* 337(1–2): 228–235.

2. Sekulic, D. P., Male, A. T., Pan, C., and Gao, F. 2001. Modeling of molten clad flow and diffusion of Si across a clad-core interface of an aluminum brazing sheet. *DVS — Berichte* 212:204–209.

3. Sekulic, D. P., Salazar, J. A., Gao, F., Rosen, S. J., and Hutchins, F. H. 2003. Local transient behavior of a compact heat exchanger core during brazing, equivalent zonal (EZ) approach. *Int. Journal of Heat Exchangers* 4(1): 91–108.

4. Braun, R. J., Murray, B. T., Boettinger, W. J., and McFadden, G. B. 1995. Lubrication theory for reactive spreading of a thin drop. *Phys. Fluids* 7(8): 1797–1809.

5. Terrill, R. J. 1966. Diffusion of silicon in aluminum brazing sheet. *Welding Journal* 45(5): 202-s to 209-s.

6. Sekulic, D. P. 2000. Molten metal micro layer prior to joint formation during brazing. A prolegomena for scaling analysis. *Proc. of the Third Int. Symp. on Scale Modeling,* Nagoya, Japan: JSME, CD edition. pp. 86–93.

7. Sigiyama, Y. 1989. Brazing of aluminum alloys. *Welding International* 8:700–710.

8. Woods, A. R., and Robinson B. I. 1974. Flow of aluminum dip brazing filler metals. *Welding Journal* 53(10): 440-s to 445-s.

9. Sekulic, D. P. 2001. Molten aluminum equilibrium membrane formed during controlled atmosphere brazing. *International Journal of Engineering Science* 39:229–241.

10. Zellmer, P. B., Nigro, N., and Sekulic, D. P. 2001. Numerical modeling and experimental verification of the formation of 2D and 3D brazed joints. *Modelling and Simulation in Materials Science and Engineering* 9:339–355.

11. Sekulic, D. P., Zellmer, P. B., and Nigro N. 2001. Influence of joint topology on the formation of brazed joints. *Modelling and Simulation in Materials Science and Engineering* 9:357–369.

12. Brakke, K. A. 1999. *Surface Evolver Manual.* Version 2.14, August 18, 1999. Available at *http://www.susqu.edu/facstaff/b/brakke/evolver/evolver.htm.*

13. Racz, L. M., Szekely, J., and Brakke, K. A. 1993. A general statement of the problem and description of a proposed method of calculation for some meniscus problems in materials processing. *ISIJ International* 33(2): 328–335.

14. Zhao, H., and Sekulic, D. P. 2003. Modeling of the influence of a microstructure scale on the re-solidification of micro layers of a molten aluminum alloy. *Proc. of the Fourth Int. Symposium on Scale Modeling — ISSM-IV*, Cleveland, Ohio. NCRM-NASA Glenn Research Center. pp. 291–301.

15. Shah, R. K., and Sekulic, D. P. 2003. *Fundamentals of Heat Exchanger Design.* Hoboken, N.J.: Wiley. p. 38.